



HAL
open science

**A new range of specific perovskite-type materials with structural, magnetic and magnetocaloric properties:
La_{0.67}Ca_{0.33}-Sr Mn_{0.98}Fe_{0.02}O₃ ($0.15 \leq x \leq 0.3$)**

K. Laajimi, F. Ayadi, M. Kchaw, I. Fourati, M. Khlifi, M.H. Gazzah, J. Dhahri, Jean Juraszek

► **To cite this version:**

K. Laajimi, F. Ayadi, M. Kchaw, I. Fourati, M. Khlifi, et al.. A new range of specific perovskite-type materials with structural, magnetic and magnetocaloric properties: La_{0.67}Ca_{0.33}-Sr Mn_{0.98}Fe_{0.02}O₃ ($0.15 \leq x \leq 0.3$). Solid State Sciences, 2021, 119, pp.106683. 10.1016/j.solidstatesciences.2021.106683 . hal-03329917

HAL Id: hal-03329917

<https://normandie-univ.hal.science/hal-03329917>

Submitted on 2 Aug 2023

HAL is a multi-disciplinary open access archive for the deposit and dissemination of scientific research documents, whether they are published or not. The documents may come from teaching and research institutions in France or abroad, or from public or private research centers.

L'archive ouverte pluridisciplinaire **HAL**, est destinée au dépôt et à la diffusion de documents scientifiques de niveau recherche, publiés ou non, émanant des établissements d'enseignement et de recherche français ou étrangers, des laboratoires publics ou privés.



Distributed under a Creative Commons Attribution - NonCommercial 4.0 International License

A new range of specific perovskite-type materials with structural, magnetic and magnetocaloric properties: $\text{La}_{0.67}\text{Ca}_{0.33-x}\text{Sr}_x\text{Mn}_{0.98}\text{Fe}_{0.02}\text{O}_3$ ($0.15 \leq x \leq 0.3$)

K. Laajimi^{a,b}, F. Ayadi^b, M. Kchaw^b, I. Fourati^b, M. Khelifi^c, M. H. Gazzah^a, J. Dhahri^c, and J. Juraszek^{b,*}

^a Laboratoire de physique quantique et statistique, Faculté des Sciences de Monastir, Université de Monastir, Avenue de l'Environnement, Monastir, 5019, Tunisie.

^b Normandie Université, UNIROUEN, INSA Rouen, CNRS, GPM, 76000 Rouen, France.

^c Laboratoire de Physique de la matière condensée et des nanosciences, Faculté des Sciences de Monastir, Université de Monastir, Avenue de l'Environnement, Monastir, 5019, Tunisie.

Abstract

The effect of strontium doping on the structural, magnetic and magnetocaloric properties of $\text{La}_{0.67}\text{Ca}_{0.33-x}\text{Sr}_x\text{Mn}_{0.98}\text{Fe}_{0.02}\text{O}_3$ samples for ($x=0.15$; 0.2 and 0.3) has been investigated. Analysis using X-ray diffraction shows there is an orthorhombic structure with $Pnma$ space group symmetry for $x = 0.15$ compound, whereas there is a rhombohedral structure exhibiting $R\bar{3}c$ space group symmetry found for $x = 0.2$, and $x = 0.3$ compounds. A second-order magnetic phase transition from ferromagnetic to paramagnetic state transition is evidenced for all samples, with Curie temperature (T_C) values equal to 329 K, 330 K and 350 K and that respectively for $x = 0.15$, 0.2 and 0.3. Based on isothermal magnetization measurements versus applied magnetic field at several temperatures around T_C , the magnetic entropy change was calculated, which is very close to that approximated by the Landau theory for $x=0.15$. Under an applied magnetic field of 5 T, one can see the maximum magnetic entropy change ($-\Delta S_M^{max}$) values, which are around 4.89, 4.71 and 3.35 $\text{J.kg}^{-1}.\text{K}^{-1}$ for $x = 0.15$, 0.2, and 0.3 respectively. It confirms that close to room temperature, these manganites are admirably potential functional materials, which can be applied as solid state magnetic refrigerants.

Keywords: Manganites, magnetocalorics, magnetic measurements, magnetic entropy.

1. Introduction

Manganites of general formula $\text{Tr}_{1-x}\text{D}_x\text{MnO}_3$ (in which Tr is a rare earth ion and D is an alkaline earth or alkaline ion) are very attractive due to their potential technological applications such as magnetocaloric cooling devices and magneto-electronic technology [1]. The magnetocaloric effect (MCE) is defined as a typical property of magnetic materials consisting of an adiabatic variation of temperature due to variations of external magnetic field [2, 3]. The nature of magnetic properties of manganites depends principally on the existence of a mixed-valence state $\text{Mn}^{3+}/\text{Mn}^{4+}$. Ferromagnetic (FM) and antiferromagnetic (AFM) interactions, which results from $\text{Mn}^{3+} - \text{Mn}^{4+}$, $\text{Mn}^{3+}-\text{Mn}^{3+}$, and $\text{Mn}^{4+}-\text{Mn}^{4+}$ ion pairs, respectively, are driven by the latter. An electron transfer that occurs between neighboring ions Mn^{3+} and Mn^{4+} through the oxygen anion O^{2-} explains the double exchange (DE) model [4]. Therefore, these electrons' spins are parallel, causing a ferromagnetic metal transition. Numerous investigations as reported in the literature have shown significant MCE values for selected manganites near room temperature [5; 6].

Among these manganites, LaMnO_3 is defined as an antiferromagnetic insulator (AFI) characterized by a super-exchange coupling (SE) between Mn^{3+} ions [7]. Substituting the A-site or the B-site can easily influence the properties of such manganite, as reported in the literature [8, 9]. Ferromagnetic metallic properties of new manganites found origin from a partial substitution of La^{3+} by divalent ions such as Ca^{2+} , Sr^{2+} , Ba^{2+} , *etc*, as explained by the Zener theory (double exchange). In comparison, $\text{La}_{0.7}\text{Ca}_{0.3}\text{MnO}_3$ exhibits a higher magnetocaloric effect (MCE) as compared to $\text{La}_{0.7}\text{Sr}_{0.3}\text{MnO}_3$, but with a reduced Curie temperature below room temperature. Doping Ca manganites with low amounts of Sr raises the Curie temperature towards ambient temperature, resulting in a significant advance toward magnetic refrigeration based applications, but at the cost of a smaller MCE [10].

Whereas $La_{1-x}Ca_xMnO_3$ ($x = 0.2, 0.33$) has a larger magnetic entropy change compared to gadolinium [11], while its Curie temperature (T_C) is 251 K, lower than 294 K for Gd [12], which makes it a promising material for magnetic refrigeration at room temperature. Furthermore, $La_{0.67}Ca_{0.33-x}Sr_xMnO_3$ has significant magnetocaloric properties [13] with $T_C=346$ K for $x = 0.25$ [14]. Significantly, increasing Sr in the compound decreases T_C closer to room temperature [15]. Substitution of A site by Sr and Ca ions affects T_C , due to the difference between the ionic radii of the two ions [16].

In the present study, we investigated the effect of A-site substitution on the structural, magnetic, and magnetocaloric properties of $La_{0.67}Ca_{0.33-x}Sr_xMn_{0.98}Fe_{0.02}O_3$ for ($x=0.15; 0.2$ and 0.3) manganites.

2. Materials and methods

Sr-doped manganites $La_{0.67}Ca_{0.33-x}Sr_xMn_{0.98}Fe_{0.02}O_3$ with ($x = 0.15; 0.2$ and 0.3) have been synthesized in air via the sol-gel method using $C_6H_9LaO_6$, H_2O , $C_4H_6CaO_4 \cdot H_2O$, N_2O_6Sr , $C_4H_6MnO_4 \cdot 4H_2O$ and Fe_2O_3 precursors. The Stoichiometric amounts of precursors were diluted in distilled water to obtain a mixed solution. Afterwards, a hot plate on which the solution was heated with stirring equal to $90^\circ C$. After complete dissolution of the precursors, the citric acid (used as complexation agent for the various metal cations) was inserted with an adequate amount. Molar ratios between the precursors and citric acid were adjusted to 1:1. The pH of the solution was changed towards 7 with ammonia addition. Subsequently, stoichiometric quantities of ethylene glycol were mixed with the solution (employed as a polymerization agent) in order to improve our sample preparation and gel transfer. The gel drying was done up to about 100 to $140^\circ C$ to have a dry foam. The produced powder produced was annealed at $600^\circ C$ for 5 hours. Subsequently, the resulting final compound was compacted to pellets and later sintered over 24 at $1000^\circ C$ to improve crystallinity.

To characterize our compounds, we performed phase purity measurements with (XRD) X-ray powder diffraction, about ambient temperature, employing a "Panalytical X pert Pro" using Cu-K α radiation ($\lambda \approx 1.7889 \text{ \AA}$). Results were obtained with 2Θ ranging between 15° and 90° , with a step size of 0.009° . Morphological analysis and energy spectrum of the compounds were performed by using a Field Emission Scanning Electron Microscope (SEM) coupled with an Energy Dispersive Spectrometer (EDX). In addition, X-ray mapping was realized with the same instrument (SEM). Magnetization was measured using a MPMS-XL SQUID magnetometer, operating in 5 K – 400 K temperature range with application of an external magnetic field reaching until 5 T.

3. Results and discussion

3.1 X-ray diffraction analysis

Figure 1(a) shows the X-ray powder diffraction patterns of polycrystalline samples $\text{La}_{0.67}\text{Ca}_{0.33-x}\text{Sr}_x\text{Mn}_{0.98}\text{Fe}_{0.02}\text{O}_3$ for ($x=0.15$; 0.2 and 0.3). From the obtained results, all the compounds have a single phase without any detectable secondary phase. The data have been refined using the standard Rietveld method using Fullprof software [17; 18; 19]. At room temperature, we have indexed the XRD data corresponding to $x = 0.15$ within a rhombohedral structure with $Pnma$ spatial group. Inside the crystal lattice, La/Ca/Sr take 4c ($x, 0.25, z$) Whycoff atomic positions, Mn/Fe are at positions 4a ($0, 0, 1/2$), O1 are at positions 4c($x, 0.25, z$) and O2 8d (x, y, z). For $x = 0.2$ and $x = 0.3$ samples, the crystalline rhombohedral structure has evolved to $R\bar{3}c$ spatial group. Within this crystalline structure, La/Ca/Sr are located at Whycoff's atomic positions 6a ($0, 0, 0.25$), Mn/Fe are present at positions 6b ($0, 0, 0$), O occur at positions 18e ($x, 0, 0.25$). Figure 1(b) shows the Rietveld refinement patterns of $x = 0.2$ sample, the results of the Rietveld refinement being reported out in Table 1. A change of the crystal structure of the samples from a low symmetric orthorhombic to a high symmetric

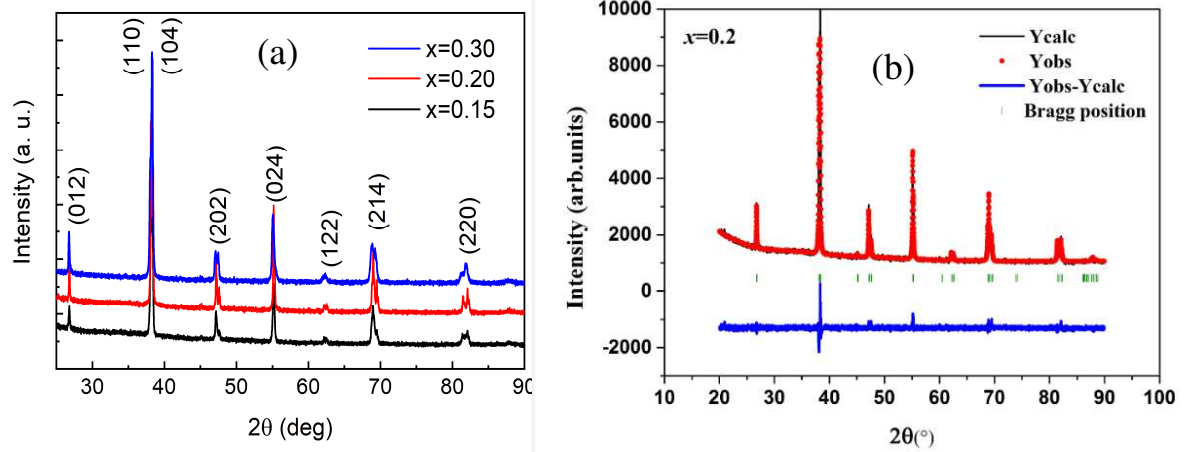


Fig. 1: (a) XRD Powder Model for $\text{La}_{0.67}\text{Ca}_{0.33-x}\text{Sr}_x\text{Mn}_{0.98}\text{Fe}_{0.02}\text{O}_3$ ($x = 0.15, 0.2$ and 0.3) compounds at room temperature. (b) Experimental (open symbols) and calculated (solid lines) XRD data for $\text{La}_{0.67}\text{Ca}_{0.33-x}\text{Sr}_x\text{Mn}_{0.98}\text{Fe}_{0.02}\text{O}_3$ ($x=0.2$). Vertical bars mark positions for the

rombohedral structure due to the increased Sr content can be seen in Table 1. This can be explained by a larger ionic radius of Sr^{2+} (1.44 \AA) as compared to Ca^{2+} (1.34 \AA), increasing the tolerance factor (t), which is defined as [20]:

$$t = \frac{r_A + r_O}{\sqrt{2}(r_{Mn} + r_O)} \quad (1)$$

Bragg reflection. Differences between the observed and the calculated intensities are shown at the bottom of the diagram.

Where r_A , r_{Mn} and r_O values are the average ionic radii of A-site, Mn ions and oxygen ions, respectively. The structures can then be classified according to the values of the tolerance factor.

If the corresponding value is equal to 1, the system has an ideal cubic structure. Rhombohedral distortions are shown, if the value of t changes between 0.96 and 1. If t is less than 0.96 [21], the Orthorhombic distortions appear. In our case, the values of tolerance factor calculated for the $\text{La}_{0.67}\text{Ca}_{0.33-x}\text{Sr}_x\text{Mn}_{0.98}\text{Fe}_{0.02}\text{O}_3$ for ($x=0.15$; 0.2 and 0.3) samples are equal to 0.9737, 0.9755 and 0.9790, respectively, so, an agreement with a rhombohedral structure.

Based on linewidth of the most intense peaks, we calculated the size of the crystallites (D), according to the following Scherrer equation [22]:

$$D = \frac{K\lambda}{\beta \cos\theta} \quad (2)$$

Where the constant K is related to the crystallite form size ($K = 0.9$), so-called shape factor), β being the full width at half maximum (FWHM), where λ represents the X-ray wavelength ($\lambda = 1.5406 \text{ \AA}$) and θ being the Bragg diffraction angle of the most intense peak (104). During the calculation of FWHM, the instrumental broadening factor was considered ($\beta = \sqrt{(\beta_{abs}^2 - \beta_{ins}^2)}$). After, the average crystallite sizes of our compound $\text{La}_{0.67}\text{Ca}_{0.33-x}\text{Sr}_x\text{Mn}_{0.98}\text{Fe}_{0.02}\text{O}_3$ for ($x=0.15$, 0.2 and 0.3) are equal to 41.9 nm, 42.4 nm and 44.3 nm respectively.

Table 1: Results of the Rietveld refinement of the $\text{La}_{0.67}\text{Ca}_{0.33-x}\text{Sr}_x\text{Mn}_{0.98}\text{Fe}_{0.02}\text{O}_3$ polycrystalline.

Parameters	$x = 0.15$	$x=0.2$	$x=0.3$
Symmetry	Orthorhombic	rhombohedral	rhombohedral
Space group	Pnma	$R\bar{3}c$	$R\bar{3}c$
a (Å)	5.449(9)	5.484(1)	5.496(4)
b (Å)	7.734(9)	5.484(1)	5.496(4)
c (Å)	5.492(6)	13.310(8)	13.350(0)
V (Å ³)	231.537(4)	346.687(1)	349.275(9)
Atoms position			
La/ Ca/Sr			
	X 0.0183(7)	0.0000(0)	0.0000(0)
	Y 0.2500(0)	0.0000(0)	0.0000(0)
	Z 0.0029(4)	0.2500(0)	0.2500(0)
Mn/Fe			
	X 0.0000(0)	0.0000(0)	0.0000(0)
	Y 0.0000(0)	0.0000(0)	0.0000(0)
	Z 0.5000(0)	0.0000(0)	0.0000(0)
O1			
	X 0.4056(7)	0.5421(0)	0.5513(7)
	Y 0.2500(0)	0.0000(0)	0.0000(0)
	Z 0.0957(7)	0.2500(0)	0.2500(0)
O2			
	X 0.3001(1)	-	-
	Y -0.0057(4)	-	-
	Z 0.7754(3)	-	-

Bond lengths and bond angles

Mn-O1-Mn (°)	138.35(2)	166.378(4)	163.420(13)
Mn-O2-Mn (°)	173.57(6)		
Mn-O1 (Å)	2.06888(19)	1.94677(4)	1.95829(11)
Mn-O2 (Å)	2.2284(11)		
Agreement factors			
R _p (%)	3.58	2.67	3.28
R _{wp} (%)	5.36	3.49	5.06
R _{exp} (%)	2.97	2.79	2.71
χ^2	3.26	1.57	3.48

3.2 Scanning electron microscope (SEM)

Figures 2 (a-c) show the SEM micrographs of nanoparticles of the compounds. The grain size increases gradually from 0.41 μm (for $x = 0.15$) up to 0.79 μm (for $x = 0.3$) (see insets of Fig. 2). In addition, it exhibits a homogeneous microstructure with a uniform particle size distribution. Compared with section 3.1, the observed grain sizes by SEM are larger than

those calculated by Scherrer's formula. This can be explained by the fact that each particle observed by SEM is formed by several crystallized grains.

The elemental mapping show the presence of elements La, Ca, Sr, Mn, Fe and O, on the surface of nanoparticles with a homogeneous distribution, as illustrated in Fig. 2.

The mean particle size was evaluated by using Digimizer and the resulting values were fitted with the following log-normal relation [23, 24]:

$$f(D) = \left(\frac{1}{\sqrt{2\pi\sigma D}} \right) \exp \left[-\frac{\ln^2\left(\frac{D}{D_0}\right)}{2\sigma^2} \right] \quad (3)$$

Where the values D_0 and σ represent the median diameter and data dispersion, respectively. The determination of the mean diameter $\langle D \rangle$ and standard deviation σ_D were derived from the results obtained by fitting through Eq. (3) and relations (4) and (5), thus the result is summarized in **Table 2**.

$$\langle D \rangle = D_0 \exp\left(\frac{\sigma^2}{2}\right) \quad (4)$$

$$\sigma_D = \langle D \rangle [\exp(\sigma^2) - 1]^{1/2} \quad (5)$$

Table 2: Crystallite and particle size of the samples.

Sample	$D_{\text{xrd}}(\text{nm})$	$D_{\text{SEM}}(\mu\text{m})$	$\sigma_D(\mu\text{m})$
$x = 0.15$	41.9	0.41	0.39
$x = 0.2$	42.4	0.68	0.41
$x = 0.13$	44.3	0.79	0.69

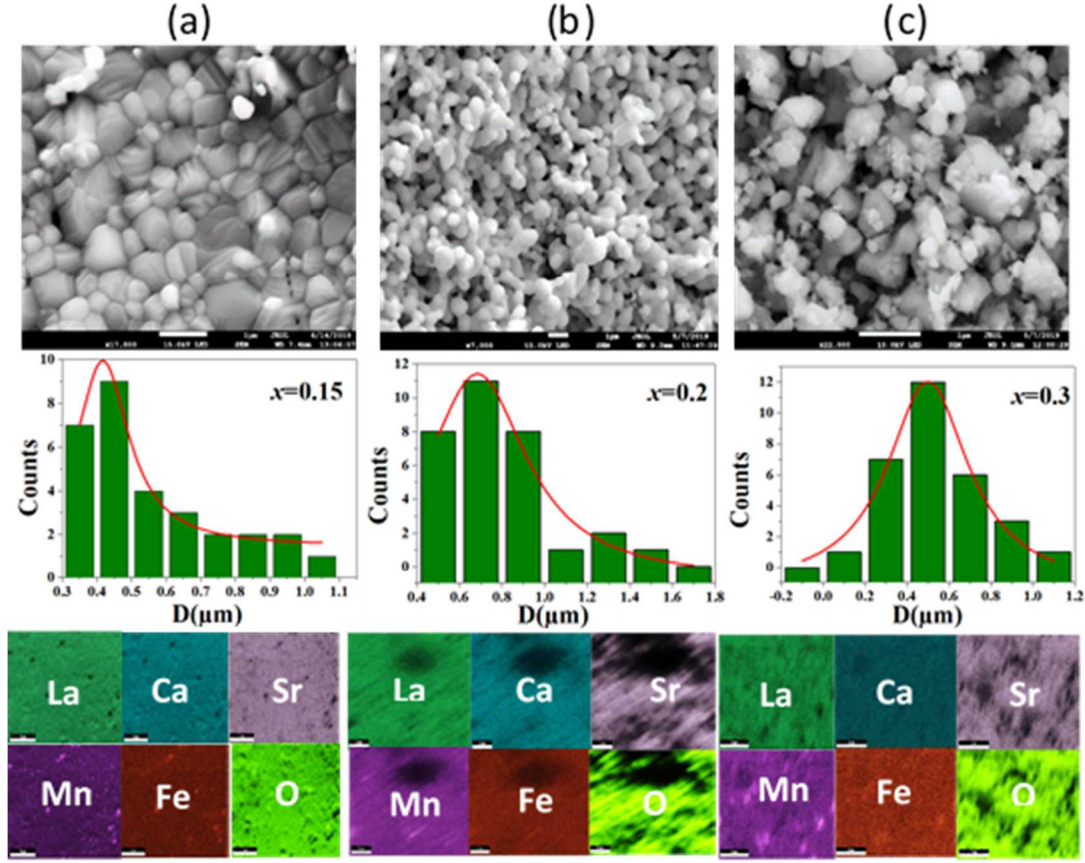
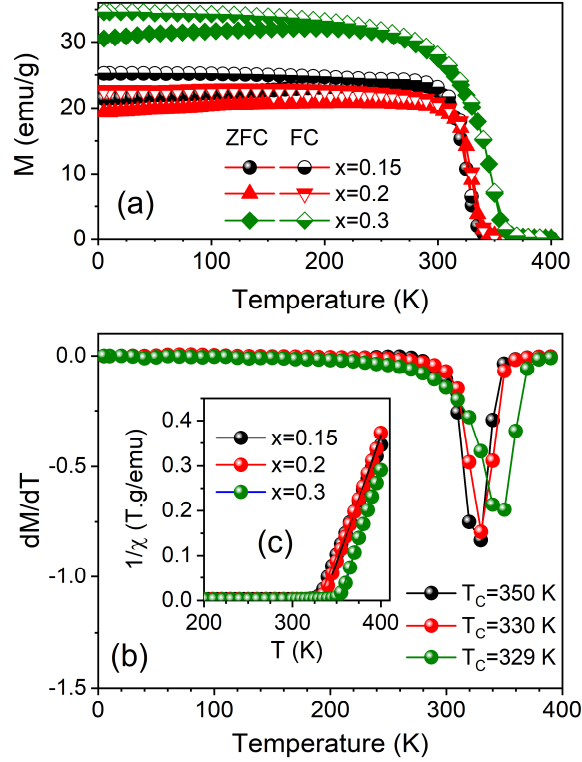


Fig. 2: Scanning electron micrographs for $\text{La}_{0.67}\text{Ca}_{0.33-x}\text{Sr}_x\text{Mn}_{0.98}\text{Fe}_{0.02}\text{O}_3$ ($x = 0.15$, 0.2 and 0.3) samples. Particle size distribution of the corresponding sample. EDX mapping of La, Ca, Sr, Mn, Fe and O elements.

3.3 Magnetic properties

Figure 3(a) displays the dependence of M-T curves at field-cooled (FC) and zero-field-cooled (ZFC) for $\text{La}_{0.67}\text{Ca}_{0.33-x}\text{Sr}_x\text{Mn}_{0.98}\text{Fe}_{0.02}\text{O}_3$ for ($x = 0.15$; 0.2 and 0.3), under an applied field value of 0.05 T. The values of magnetization are quite stable at temperatures below 290 K for $x = 0.15$, 295 K for $x = 0.2$ and 300 K for $x = 0.3$, and vanish at temperature close to the critical temperature, T_c . Therefore, a clear magnetic transition from ferromagnetic to paramagnetic state appears in all samples [Fig. 3(a)].

The irreversibility between the ZFC and FC magnetization curves at 0.05 T is low and close to T_c in all samples. This thermomagnetic irreversibility phenomenon arises from magnetic anisotropy, which results from the difference between measuring FC and ZFC on polycrystalline samples. Under T_c temperature, the magnitude of ZFC magnetization will be



dependent on anisotropy, and consequently a greater difference between FC and ZFC magnetizations will be present for highly anisotropic samples. Which means that the irreversibility between FC and ZFC magnetizations in ferro and ferrimagnetic systems are the result of their magnetic anisotropy and not of Spin Glass behavior. This phenomenon has been observed in many ordered magnetic systems [25, 26].

In figure 3 (b), we plotted the inflection point of dM/dT from which we have determined all the values of T_C ($T_C = 329, 230$ and 350 K for $x = 0.15, 0.2$ and $x = 0.3$, respectively), (For more information, refer to Table 2). Following the increase of Sr content, Curie temperature T_C increases gradually due to the continuous structural distortion through the Sr perovskite structure. As evidenced by the increase of A-site, disorder σ_2 and average ion radius $\langle r_A \rangle$ increases progressively. From $M(T)$ curves, we deduce the inverse of susceptibility, which obeys the Curie Weiss-Law [27; 28]:

Fig. 3: (a) Variations of ZFC and FC magnetization as a function of temperature for $\text{La}_{0.67}\text{Ca}_{0.33-x}\text{Sr}_x\text{Mn}_{0.98}\text{Fe}_{0.02}\text{O}_3$ ($x = 0.15, 0.2$ and 0.3) samples exposed to a magnetic field strength of 0.05 T. (b) Field cooling curve differential ($dM-dT$) from which the phase-transition temperature T_C was determined. (c) Inset shows the inverse of susceptibility vs. temperature at $\mu_0H = 0.05\text{T}$.

$$\chi(T) = \frac{C}{(T-\theta_p)} \quad (6)$$

From the interception of the curve $1/\chi$ with the temperature axis, the Curie-Weiss temperature (θ_p) was deduced, and, the Curie constant (C) was established from the slope of the linear $1/\chi$ vs. T curve Fig. 3 (c). Based on the Curie constant, we determined the values of the effective paramagnetic moment (μ_{eff}^{exp}) according to the following relation [27; 29]:

$$\mu_{eff}^{exp} = \sqrt{\frac{3Ck_B M_m}{N_a}} \mu_B \quad (7)$$

Where $\mu_B = 9.274 \times 10^{-21} \text{A.m}^2$ is the the Bohr magneton; $N_a = 6.022 \times 10^{23} \text{mol}^{-1}$ is the Avogadro number; $k_B = 1.380649 \times 10^{-23} \text{J k}^{-1}$ is the Boltzmann constant; and M_m represents the molecular mass. Nonetheless, the determination of theoretical effective moments in units of Bohr magneton of $\text{La}_{0.67}\text{Ca}_{0.33-x}\text{Sr}_x\text{Mn}_{0.98}\text{Fe}_{0.02}\text{O}_3$ was performed using the following formula [30]:

$$\mu_{eff}^{the} = \sqrt{0.63 \times \mu_{eff}^2(\text{Mn}^{3+}) + 0.35 \times \mu_{eff}^2(\text{Mn}^{4+}) + 0.02 \times \mu_{eff}^2(\text{Fe}^{2+})} \quad (8)$$

Where $\mu_{eff}^{the} = 6.70 \mu_B$ for Fe^{2+} , $\mu_{eff}^{the} = 4.90 \mu_B$ for Mn^{3+} and $\mu_{eff}^{the} = 3.87 \mu_B$ for Mn^{4+} [31].

The values of T_C , θ_p , μ_{eff}^{the} and μ_{eff}^{exp} are summarized in Table 2. The positive values of θ_p confirms the ferromagnetic behavior of all samples, and the decrease of θ_p with x follows the T_C tendency. We also note a certain difference in values of theoretical and experimental effective moments. The reason for this difference lies in the presence of a short-range

Table 2: Temperature of transition T_c , temperature of Curie-Weiss θ , experimental μ_{eff}^{exp} and theoretical μ_{eff}^{the} paramagnetic moments for $\text{La}_{0.67}\text{Ca}_{0.33-x}\text{Sr}_x\text{Mn}_{0.98}\text{Fe}_{0.02}\text{O}_3$ compounds.

x	$T_c(\text{K})$	$\theta(\text{K})$	$\mu_{eff}^{exp}(\mu_B)$	$\mu_{eff}^{the}(\mu_B)$
0.15	329	331	5.736	4.611
0.2	330	334	5.369	4.611
0.3	350	354	5.163	4.611

magnetic order in the paramagnetic state, which is widely found in polycrystalline manganites.

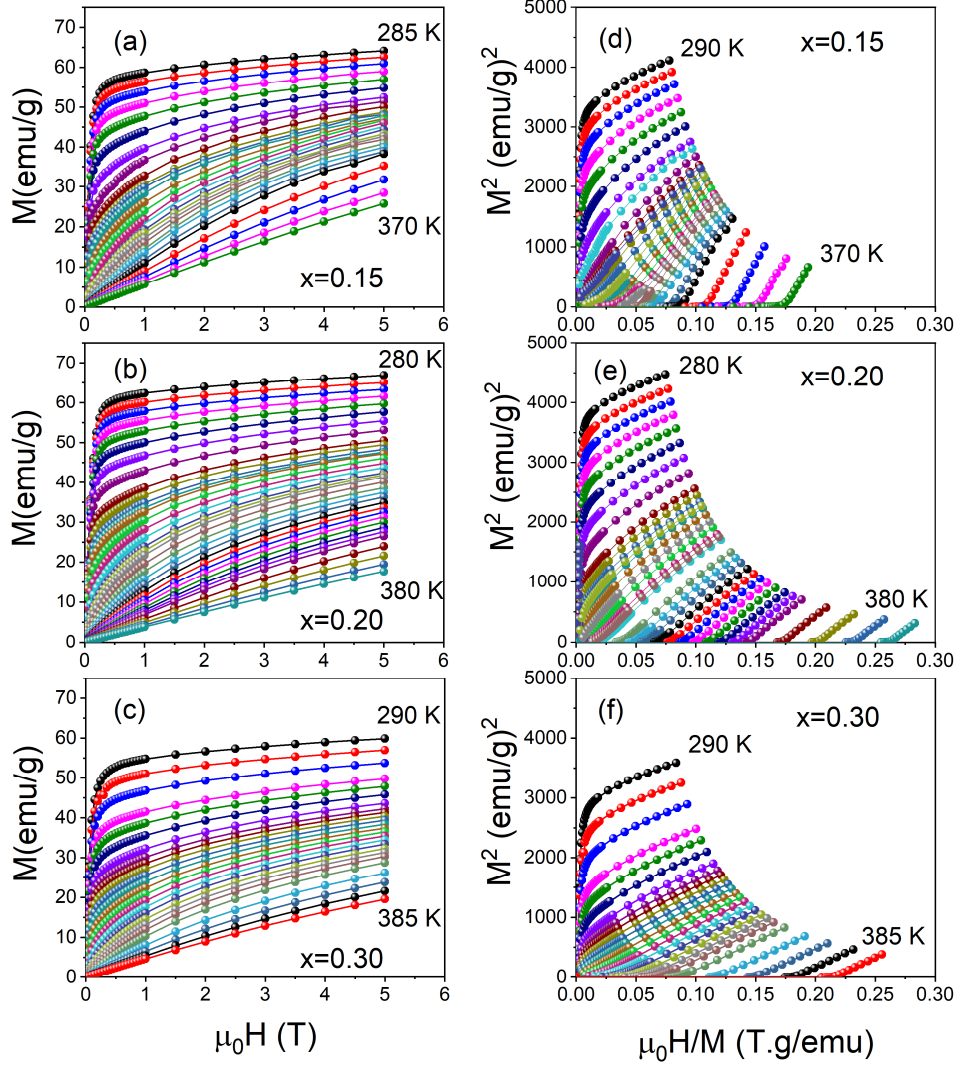


Fig. 4: (a-c) Magnetic isotherms $M(\mu_0H, T)$ for the samples $\text{La}_{0.67}\text{Ca}_{0.33-x}\text{Sr}_x\text{Mn}_{0.98}\text{Fe}_{0.02}\text{O}_3$ ($x = 0.15, 0.2$ and 0.3). (d-f) Arrott plots M^2 versus (μ_0H/M) for the samples $\text{La}_{0.67}\text{Ca}_{0.33-x}\text{Sr}_x\text{Mn}_{0.98}\text{Fe}_{0.02}\text{O}_3$ ($x = 0.15, 0.2$ and 0.3).

In order to understand the magnetic behavior of our compounds, the variation of the magnetization depending on the magnetic applied field is shown in Figs. 4(a-c) for different temperatures. At low temperatures, the ferromagnetic behavior of our samples is validated, with a strong increase of magnetization for the low values of H followed by a plateau-like behavior for fields above 1 T. Nevertheless, at high temperature, $M(H)$ curves become linear, which corresponds to paramagnetic behavior of these materials.

In order to check the order of the FM - PM transition, Figures 4(d-f) display the Arrott plots for $x = 0.15$, $x = 0.2$ and $x = 0.3$ at the temperatures between 280 to 385 K. In the high field region, a positive slope is observed for all compounds, indicating that the magnetic transition is of second-order type according to the Banerjee criterion [32]. Such criterion has

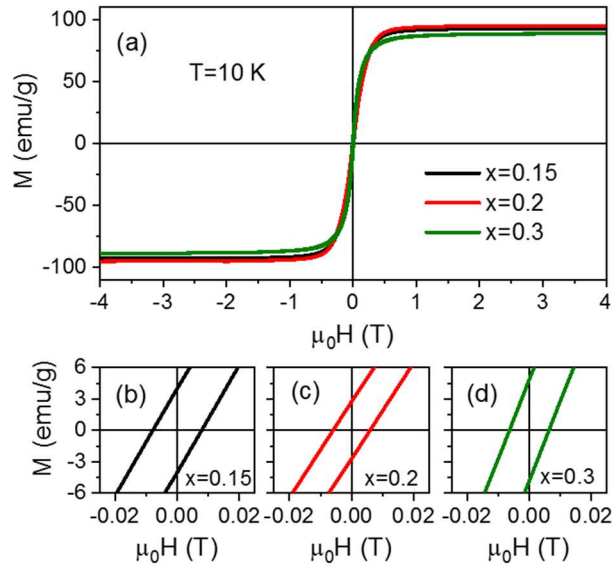


Fig. 5: (a) The hysteresis loops of the $\text{La}_{0.67}\text{Ca}_{0.33-x}\text{Sr}_x\text{Mn}_{0.98}\text{Fe}_{0.02}\text{O}_3$ ($x = 0.15, 0.2$ and 0.3) samples measured at 10 K temperature. (b-d) Zoom of hysteresis loops in low magnetic field regions at 10 K for the different x values.

also been used for other manganites [33].

In Fig. 5(a), we presented the hysteresis cycles at 10 K for $\text{La}_{0.67}\text{Ca}_{0.33-x}\text{Sr}_x\text{Mn}_{0.98}\text{Fe}_{0.02}\text{O}_3$ compounds. The magnetization curves are quite similar with a small hysteresis loop, the ferromagnetic state at lower temperature being confirmed by the saturation of M at around $\mu_0 H = 0.5$ T. The values of the saturation magnetization (M_S) determined at 10 K are 92.14 and 94.49 and 88.75 emu/g, for $x=0.15, 0.2$ and 0.3 , respectively. A zoom of the central

portion of the $M(\mu_0H)$ curves in a low magnetic field value is shown in Figs. 5 (b-d) for the different compositions. The μ_0H_C values are 73×10^{-4} T, 60×10^{-4} T and 63×10^{-4} T, for $x = 0.15$, 0.2 and 0.3, respectively. The M_r values are 3.96, 2.71 and 4.83 emu/g, for $x = 0.15$, 0.2 and 0.3, respectively. Therefore, a typical soft FM behavior is found for our materials, with low values of coercive field (μ_0H_C) and remanant magnetization (M_r). Our compounds can then find application for writing and reading process in high-density registration media or storage of information [34].

In the following, we calculate the magneto-crystalline anisotropy, which is an intrinsic property of materials, and plays a significant role in coercivity [35]. The determination of the anisotropy constant (K_a) is based on Stoner-Wohlfarth's theory, from Eq. 6 [36]:

$$\mu_0H_C = (0.98 \times K_a)/M_s \quad (9)$$

Where K_a values are 0.686 J.m^{-3} , 0.578 J.m^{-3} and 0.570 J.m^{-3} , for $x = 0.15$, 0.2 and 0.3, respectively. The remanence ratio (R) was calculated according to Eq. 7:

$$R = M_r/M_s \quad (10)$$

We obtained R values of 0.043 and 0.028 and 0.054 for $x = 0.15$, 0.2 and 0.3, respectively. These low remanence ratios verify that the magnetic properties of our materials are isotropic [37].

3.4 Magnetocaloric properties

By definition, the magnetocaloric effect (MCE) is an intrinsic property of magnetic materials. It represents the material's reaction to the application or suppression of magnetic field [38]. Based on the thermodynamic theory, MCE is derived from Maxwell thermodynamic relation [39]:

$$\left(\frac{\partial S}{\partial(\mu_0H)} \right)_T = \left(\frac{\partial M}{\partial T} \right)_{\mu_0H} \quad (11)$$

The magnetic entropy change ΔS_M , resulting from the spin ordering and caused by the change of the applied magnetic field between 0 and H_{max} , can be calculated using the following equation:

$$\Delta S_M(T, \mu_0 H) = S_M(T, \mu_0 H) - S_M(T, 0) = \int_0^{\mu_0 H_{max}} \left(\frac{\partial M}{\partial T} \right)_{\mu_0 H} d(\mu_0 H) \quad (12)$$

The calculation of the isothermal magnetic entropy change of our compounds at various temperatures near T_C , was performed by approximating equation Eq. (12) with the following functional equation [40]:

$$-\Delta S_M(T, \Delta \mu_0 H) = \sum_i \frac{M_{i+1}(T_{i+1}, \mu_0 H_{i+1}) - M_i(T_i, \mu_0 H_i)}{T_{i+1} - T_i} \quad (13)$$

Where M_i and M_{i+1} represent the experimental measured magnetization values at T_i and T_{i+1} , respectively, under an applied magnetic field fixed $\mu_0 H_i$.

Using the initial magnetization isothermals versus the applied magnetic field, the magnetic entropy change (ΔS_M) was calculated for the three specimens versus temperature for various applied magnetic fields. The results are presented on the three-dimensional (3D) images in Figures 6 (a), (b) and (c). The magnetic entropy change (ΔS_M) varies with the applied magnetic field and temperature, with a maximum value (ΔS_M^{max}) reached for a temperature close to T_C . The evolution of ΔS_M vs T for $\mu_0 H = 5$ T is shown in Fig. 6 (d) for all compounds. Obtained values of the maximum of ΔS_M (see table 3) are higher than those reported for other manganites, such as $\text{La}_{0.67}\text{Ca}_{0.33}\text{MnO}_3$ [43], indicating that our materials are very interesting for magnetocaloric applications above room temperature [44].

The magnetic refrigeration performance provided by the materials is also dependent on the relative cooling power (RCP) that is calculated based on [45]:

$$RCP = |\Delta S_M^{max}| \times \delta T_{FWHM} \quad (14)$$

Where δT_{FWHM} is the total width at half-maximum δ_{FWHM} of the thermal evolution of ΔS_M .

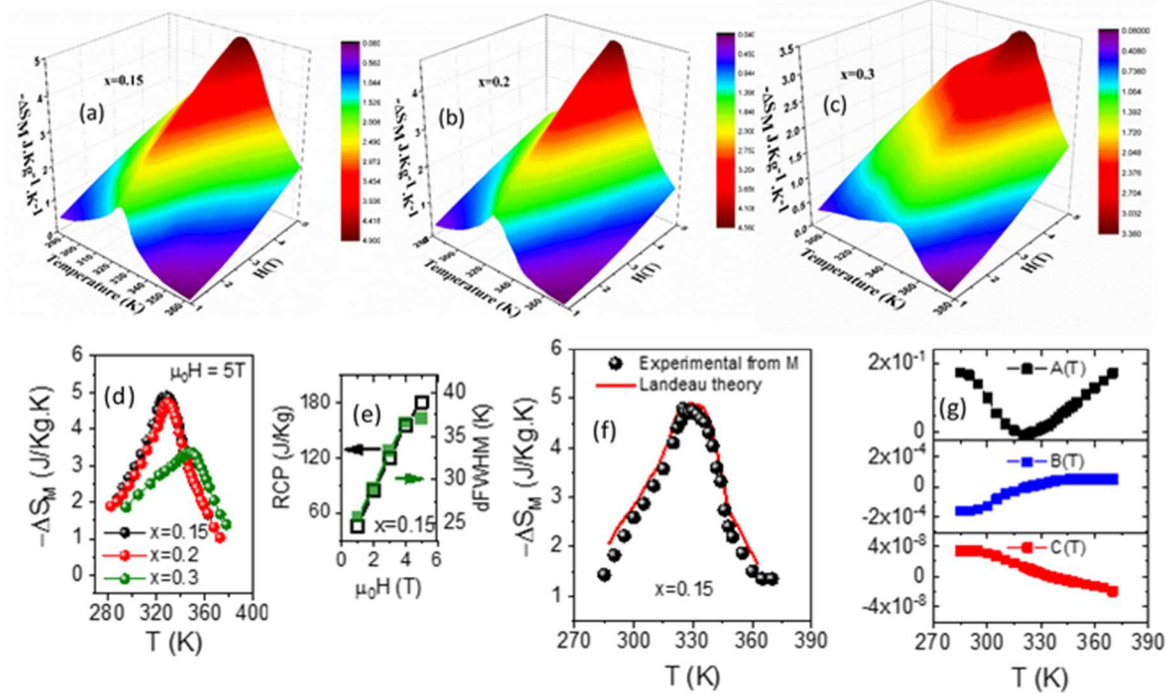


Fig. 6: (a, b and c) Temperature dependence of the magnetic entropy change at different amplitudes of the change in the applied magnetic field for the $\text{La}_{0.67}\text{Ca}_{0.33-x}\text{Sr}_x\text{Mn}_{0.98}\text{Fe}_{0.02}\text{O}_3$ ($x = 0.15, 0.2$ and 0.3) samples. (d) Temperature dependence of the maximum magnetic entropy change $-\Delta S_M$ at $\mu_0 H = 5T$ for the $\text{La}_{0.67}\text{Ca}_{0.33-x}\text{Sr}_x\text{Mn}_{0.98}\text{Fe}_{0.02}\text{O}_3$ ($x = 0.15, 0.2$ and 0.3) compounds. (e) The relative cooling power RCP and the δ_{FWHM} as a function of the variation of the applied magnetic field $\mu_0 H$. (f) Experimental and theoretical magnetic entropy change (ΔS_M) at magnetic field of 5 T ($x=0.15$). (g) Variation of Landau coefficients $A(T)$, $B(T)$ and $C(T)$ versus temperature.

The δ_{FWHM} and RCP values for the $\text{La}_{0.67}\text{Ca}_{0.33-x}\text{Sr}_x\text{Mn}_{0.98}\text{Fe}_{0.02}\text{O}_3$ sample have a linear dependence with the applied magnetic field [Fig. 6 (e)]. Subsequently, we use Landau's second-order phase transition theory for explaining the magnetic entropy change [46], assuming a mean field approximation. We can then express the Gibb's free energy as follows:

$$G(M, T) = G_0 + \frac{A(T)}{2}M^2 + \frac{B(T)}{4}M^4 + \frac{C(T)}{6}M^6 + \dots - \mu_0HM \quad (15)$$

Where $A(T)$, $B(T)$ and $C(T)$ represent the temperature dependent parameters, which contain the electron-electron interaction and the magnetoelastic coupling information [47]. The magnetic equation of state is derived from energy minimization in the following equation:

$$\mu_0H = A(T)M + B(T)M^3 + C(T)M^5 \quad (16)$$

From experimental isothermal magnetization measurements, the $A(T)$, $B(T)$ and $C(T)$ parameters are originating from polynomial fit of M versus μ_0H . In this case, we can then compute the magnetic entropy by differentiating the magnetic part of free energy:

$$S_M(T, H) = -\left(\frac{\partial F}{\partial T}\right)_H = -\frac{1}{2}A'(T)M^2 - \frac{1}{4}B'(T)M^4 - \frac{1}{6}C'(T)M^6 \quad (17)$$

Where $A'(T)$, $B'(T)$ and $C'(T)$ are the derivatives of the Landau coefficients.

The theoretical $-\Delta S_M$ values calculated from $A(T)$, $B(T)$ and $C(T)$ parameters using Eq. (17) show a good agreement with the experimental values [Figs. 6 (f-g)].

Table 3. Summary of the magnetocaloric properties of $\text{La}_{0.67}\text{Ca}_{0.33-x}\text{Sr}_x\text{Mn}_{0.98}\text{Fe}_{0.02}\text{O}_3$ compared with other various magnetic materials.

Composition References	$-\Delta S_M^{max} (J.Kg^{-1}.k^{-1})$	RCP $(J.Kg^{-1})$
	$\Delta H = 5T$	
$\text{La}_{0.67}\text{Ca}_{0.18}\text{Sr}_{0.15}\text{Mn}_{0.98}\text{Fe}_{0.02}\text{O}_3$	4.889	181 This work
$\text{La}_{0.67}\text{Ca}_{0.13}\text{Sr}_{0.2}\text{Mn}_{0.98}\text{Fe}_{0.02}\text{O}_3$	4.712	204 This work
$\text{La}_{0.67}\text{Ca}_{0.03}\text{Sr}_{0.3}\text{Mn}_{0.98}\text{Fe}_{0.02}\text{O}_3$	3.355	179 This work
Gd	9.500	410 [41]
$\text{La}_{0.7}\text{Ca}_{0.10}\text{Sr}_{0.2}\text{MnO}_3$	6.970	369 [42]
$\text{La}_{0.67}\text{Ca}_{0.33}\text{MnO}_3$	2.06	175 [43]

Conclusion

In summary, the structure, magnetic and magnetocaloric properties of $\text{La}_{0.67}\text{Ca}_{0.33-x}\text{Sr}_x\text{Mn}_{0.98}\text{Fe}_{0.02}\text{O}_3$ manganites have been investigated for ($x=0.15$; 0.2 and 0.3). The crystal structure of all samples was obtained from Rietveld's refinements of the X-ray diffraction spectra. The $x = 0.15$ compound exhibits an orthorhombic structure with the $Pnma$ space group, whereas the structure of $x = 0.2$ and $x = 0.3$ compounds is rhombohedral with the $R\bar{3}c$ space group. All compound have soft ferromagnetic properties with a Curie temperature increasing from 329 K to 350 K as Sr content inscreases. From the Arrott plots (M^2 vs. H/M) around T_C , a second order magnetic phase transition is evidenced. The values of $(-\Delta S_M^{max})$

under an applied magnetic field of 5 T are around 4.889, 4.712 and 3.355 J.kg⁻¹.K⁻¹ for $x = 0.15$, 0.2, and 0.3, respectively. In addition, we have established the relative cooling power RCP which ranges from 180.952 and 178.610 J kg⁻¹. The high magnetocaloric performance of our produced samples, with magnetic phase transition temperature just above room temperature, make these materials ideal candidates for magnetic refrigeration close to ambient.

Acknowledgments

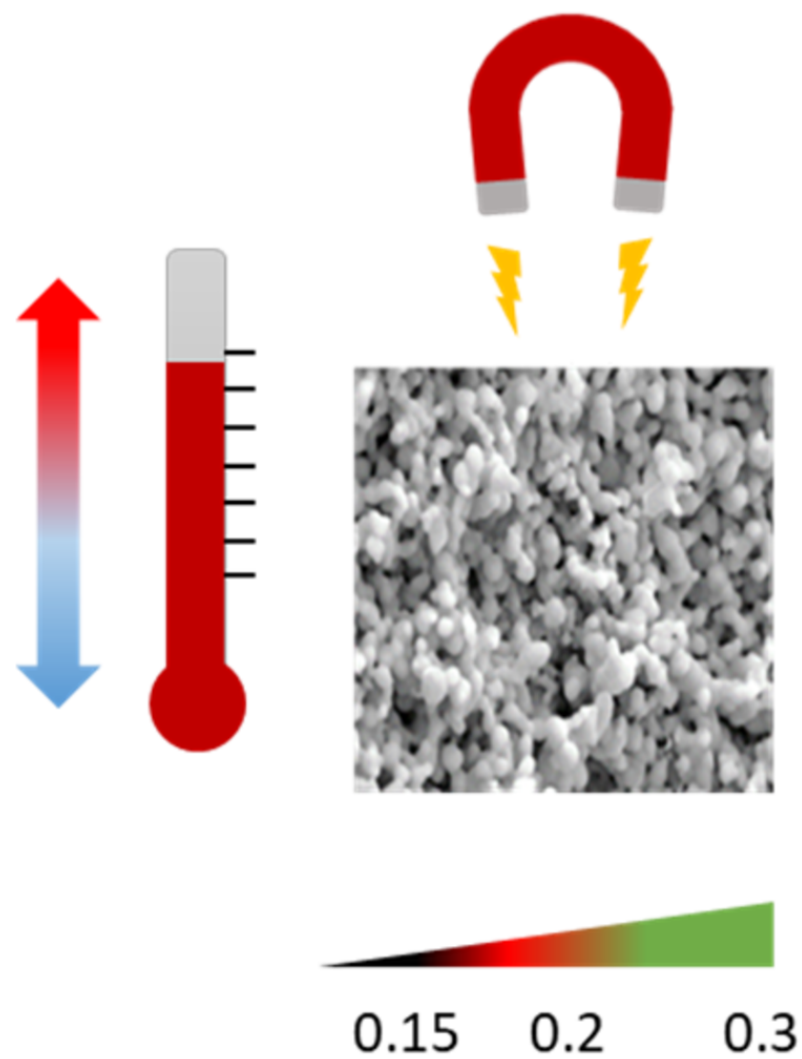
K.J is grateful for the financial support from the Tunisian Ministry of Higher Education and Scientific Research for a travelling scholarship. Region of Normandy and the European Regional Development Fund of Normandy (ERDF) in the frame of the MAGMA project supported this work.

References

- [1] S. Mahjoub, M. Baazaoui, E.K. Hlil, M. Oumezzine, *Ceram. Int.* 41 (2015) 12407–12416, <https://doi.org/10.1016/j.ceramint.2015.06.078>.
- [2] A. Selmi, R. M'nassri, W. Cheikhrouhou-Koubaa, N.C. Boudjada, A. Cheikhrouhou, *Ceram. Int.* 41 (2015) 7723–7728. <https://doi.org/10.1016/j.ceramint.2015.02.103>.
- [3] J.M.D. Coey, M. Viret, S. von Molnar, *Adv. Phys.* 48 (1999) 167, <https://doi.org/10.1080/000187399243455>.
- [4] C. Zener, *Phys. Rev* 82 (1951) 403, <https://doi.org/10.1103/PhysRev.82.403>.
- [5] M.-H. Phan, S.-C. Yu, *J. Magn. Mater.* 308 (2007) 325–340, <https://doi.org/10.1016/j.jmmm.2006.07.025>.
- [6] K. Laajimi, M. Khelifi, E. K. Hlil, M. H. Gazzah, Mossaad Ben Ayed, Hafedh Belmabrouk, J. Dhahri, *J. Mater. Sci.: Mater. Electron.* 31 (2020) 15322–15335, <https://doi.org/10.1007/s10854-020-04096-x>.
- [7] A. Elghoul, A. Krichene, N.C. Boudjada, W. Boujelben, *Ceram. Int.* 44 (2018) 12723–12730, <https://doi.org/10.1016/j.ceramint.2018.04.075>.
- [8] R. Thaljaoui, M. Pȩkała, J.-F. Fagnard, PhVanderbemden, *J. Rare Earths.* 35 (2017) 875.
- [9] S. Vadnala, P. Pal, S. Asthana, *J. Rare Earths.* 33 (2015) 1072.
- [10] María E. Botello-Zubiate, María C. Grijalva-Castillo, Daniel Soto-Parra, Renee J. Sáenz-Hernández, Carlos R. Santillán-Rodríguez and José A. Matutes-Aquino, *J. Mater.* 12 (2019) 309.
- [11] S. A. Palomares-Sánchez, S. A. Palomares-Sánchez, J. T. Elizalde Galindo, M. Mirabal-Garcia, *J. Supercond. Nov. Magn.* 28 (2015) 1635–1638. <https://doi.org/10.1007/s10948-014-2932-2>.
- [12] S. Yu. Dan'kov, A. M. Tishin, V. K. Pecharsky, and K. A. Gschneidner, Jr, *Phys. Rev. B.* **57** (1998) 3478. <https://doi.org/10.1103/PhysRevB.57.3478>.
- [13] Jeong, Y.S., Anwar, M.S., Ahmed, F., Lee, S.R., Koo, B.H, *Trans Tech Publ.* 378 (2013) 225-229. <https://doi.org/10.4028/www.scientific.net/AMM.378.225>.
- [14] D. Kim, B. L. Zink, F. Hellman, and J. M. D. Coey, *Phys. Rev. B.* 65 (2002) 214424. <https://doi.org/10.1103/PhysRevB.65.214424>.
- [15] Dhahri, A., Jemmali, M., Dhahri, E., Valente, M.A, *J. Alloy Compd.* 638 (2015) 221–227. <http://dx.doi.org/10.1016/j.jallcom.2015.01.314>.

- [16] E. L. Hernández-González, B. E. Watts, S. A. Palomares-Sánchez, J. T. Elizalde Galindo, M. Mirabal-García, *J Supercond Nov Magn* 29 (2016) 2421–2427. <https://doi.org/10.1007/s10948-016-3560-9>.
- [17] R.A. Young, *The Rietveld Method* (Oxford University Press, New York, 1993), J. Rodriguez- Carvajal, *FULLPROF* (LLB Saclay, France, 2001).
- [18] Z. Raddaoui, R. Lahouli, S. El Kossi, H. Belmabrouk, A. Bajahzar, *J. Mater. Sci.: Mater. Electron.* 31 (2020) 4836–4849, <https://doi.org/10.1007/s10854-020-03046-x>.
- [19] Z. Raddaoui, R. Lahouli, S. El Kossi, K. Khirouni, K. Taibi, *J. Alloys Compd.* 765 (2018) 428–436, <https://doi.org/10.1016/j.jallcom.2018.06.180>.
- [20] G. Xiao, W. He, P. Chen, X. Wu, *Physica B: Condensed Matter* 564 (2019) 133–142, <https://doi.org/10.1016/j.physb.2019.04.008>.
- [21] Z. Wang, Q. Xu, K. Chen, *Current Applied Physics.* 12 (2012) 1153–1157, <https://doi.org/10.1016/j.cap.2012.02.039>.
- [22] A. Taylor, *X-ray Metallography*, John Wiley & Sons Inc, New York, 993 (1961).
- [23] B. Aslibeiki, P. Kameli, M. H. Ehsani, *Ceramics International* 42.11 (2016) 12789–12795. <https://doi.org/10.1016/j.ceramint.2016.05.041>.
- [24] G.C. Lavorato, E. Lima Jr, D. Tobia, D. Fiorani, D. Troiani, H.E. Zysler, E.L. Winkler, *Nanotechnology* 25.35 (2014) 355704. <https://doi.org/10.1088/0957-4484/25/35/355704>.
- [25] J.A. Mydosh, *Spin Glasses—an Experimental Introduction*, Taylor & Francis, London, 1993.
- [26] A. Maignan, U.V. Varadara ju, F. Millange, B. Raveau, *J. Magn. Mang. Mater.* 168 (1997) 237, [https://doi.org/10.1016/S0304-8853\(97\)00006-1](https://doi.org/10.1016/S0304-8853(97)00006-1).
- [27] S. Banik, I. Das, *J. Alloys Compd.* 742 (2018) 248–255, <https://doi.org/10.1016/j.jallcom.2018.01.295>.
- [28] K. Laajimi, M. Khlifi, E.K. Hlil, M. H. Gazzah, J. Dhahri, *J. Magn. Magn. Mater.* 491 (2019) 165625, <https://doi.org/10.1016/j.jmmm.2019.165625>.
- [29] K. Laajimi, M. Khlifi, E. K. Hlil, K. Taibi, M. H. Gazzah, J. Dhahri, *J Mater Sci : Mater Electron.* 30 (2019) 11868–11877, <https://doi.org/10.1007/s10854-019-01510-x>.
- [30] S. Ghodhbane, A. Dhahri, N. Dhahri, E.K. Hlil, J. Dhahri, *J. Alloys Compd.* 550 (2013) 358–364, <https://doi.org/10.1016/j.jallcom.2012.10.087>.
- [31] X. S. Ge, Z. Z. Li, W. H. Qi, D. H. Ji, G. D. Tang, L. L. Ding, J. J. Qian, and Y. N. Du, *AIP Advances*, 7 (2017) 125002, <https://doi.org/10.1063/1.5008978>.
- [32] S. K. Banerjee, *Phys. Letters.* 12 (1964) 16. Citation: 10.1103/PhysRevLett.12.16.

- [33] J. Mira, J. Rivas, F. Rivadulla, C. Vazquez-Vazquez, M. A. Lopez-Quintela, *Phys. Rev. B.* 60 (1999) 2998, <https://doi.org/10.1103/PhysRevB.60.2998>.
- [34] K. El Maalam, M. Ben Ali, H. El Moussaoui, O. Mounkachi, M. Hamedoun, R. Masrour, E. K. Hlil, A. Benyoussef, *J. Alloys Compd.* 622 (2015) 761–764, <https://doi.org/10.1016/j.jallcom.2014.10.152>.
- [35] S. S. Nair, M. Mathews, P. A. Joy, S. D. Kulkarni, M. R. Anantharaman, *J. Magn. Magn. Mater.* 283 (2004) 344–352, <https://doi.org/10.1016/j.jmmm.2004.06.055>.
- [36] S. J. Haralkar, R. H. Kadam, S. S. More, S. E. Shirsath, M. L. Mane, S. Patil, D. R. Mane, *Phys. B.* 407 (2012) 4338–4346, <https://doi.org/10.1016/j.physb.2012.07.030>.
- [37] S. Thankachan, B. P. Jacob, S. Xavier and E. M. Mohammed, *Phys. Scr.* 87 (2013) 1–7, <https://doi.org/10.1088/0031-8949/87/02/025701>.
- [38] M. Dhahri, A. Zaidi, K. Cherif, J. Dhahri, E.K. Hlil, *J. Alloys Compd.* 691(2017) 578–586, <https://doi.org/10.1016/j.jallcom.2016.08.268>.
- [39] A.H. Morrish, *The Physical Principles of Magnetism* Wiley, New York (Chapter 3) (1965).
- [40] M. Foldeaki, R. Chahine, T.K. Bose, *J. Appl. Phys.* 77 (1995) 3528–3537, <https://doi.org/10.1063/1.358648>.
- [41] Jha, Singh, S.K., Kumar, A., Awana, V.P, *J. Magn. Magn. Mater.* 324 (2012)2849, <https://doi.org/10.1016/j.jmmm.2012.04.026>.
- [42] M.H. Phan, S.C. Yu, N.H. Hur, *Appl. Phys. Lett.* 86 (2005) 072504, <https://doi.org/10.1063/1.1867564>.
- [43] D. T. Morelli, A. M. Mance, J. V. Mantese and A. L. Micheli, *J. Appl. Phys.* 79 (1996) 373, <https://doi.org/10.1063/1.360840>.
- [44] A. Rostamnejadi, M. Venkatesan, P. Kameli, H. Salamati, J. M. D. Coey, *J. Magn. Magn. Mater.* 323 (2011) 2214–2218, <https://doi.org/10.1016/j.jmmm.2011.03.036>.
- [45] K.A. Gschneidner, V.K. Pecharsky, *Magnetocaloric Materials*, *Annu. Rev. Mater. Sci.* 30 (2000) 387–429, <https://doi.org/10.1146/annurev.matsci.30.1.387>.
- [46] L. D. Landau and E. M. Lifshitz, *Statistical Physics*, (Pergamon, New York, 1958) (1958).
- [47] V. S. Amaral and J. S. Amaral, *J. Magn. Magn. Mater.* 2104 (2004) 272–276, <https://doi.org/10.1016/j.jmmm.2003.12.870>.



Strontium
at. fraction

$-\Delta S_M$ (J/Kg.K)

